Acta Pharmaceutica Sinica B 2020;10(7):1331−1346

Chinese Pharmaceutical Association
Institute of Materia Medica, Chinese Academy of Medical Sciences

Acta Pharmaceutica Sinica B

www.elsevier.com/locate/apsb
www.sciencedirect.com

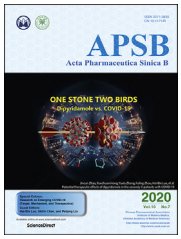

ORIGINAL ARTICLE

Novel approach for real-time monitoring of carrier-based DPIs delivery process *via* pulmonary route based on modular modified Sympatec HELOS

Xuejuan Zhang[a,b,†], Yingtong Cui[a,†], Ruifeng Liang[a], Guanlin Wang[a], Xiao Yue[a], Ziyu Zhao[a,d], Zhengwei Huang[a], Ying Huang[a,c,*], Jianfang Geng[e], Xin Pan[a,*], Chuanbin Wu[a]

[a]*School of Pharmaceutical Sciences, Sun Yat-Sen University, Guangzhou 510006, China*
[b]*Institute for Biomedical and Pharmaceutical Sciences, Guangdong University of Technology, Guangzhou 510006, China*
[c]*School of Pharmaceutical Science, Jinan University, Guangzhou 510006, China*
[d]*Department of Pharmacology, Zhongshan School of Medicine, Sun Yat-Sen University, Guangzhou 510080, China*
[e]*Sympatec GmbH Suzhou Rep. Office, Suzhou 215123, China*

Received 6 December 2019; received in revised form 12 February 2020; accepted 18 February 2020

KEY WORDS

Dry powder inhalation;
Pulmonary delivery process;

Abstract An explicit illustration of pulmonary delivery processes (PDPs) was a prerequisite for the formulation design and optimization of carrier-based DPIs. However, the current evaluation approaches for DPIs could not provide precise investigation of each PDP separately, or the approaches merely used a simplified and idealized model. In the present study, a novel modular modified Sympatec HELOS

Abbreviations: ACI, Anderson Cascade Impactor; APIs, active pharmaceutical ingredients; *a*, acceleration; CFD-DEM, computational fluid dynamics-discrete element method; CIA, cascade impactor analysis; C_{opt}, optical concentration; DPIs, dry powder inhalations; d_{ae}, aerodynamic diameter; dQ_3, the volume percentage of particles within certain range; ED, emitted dose; EDXS, energy-dispersive X-ray spectroscopy; FPF, fine particle fraction; FPD, fine particle dose; F_C, centrifugal force; F_D, drag force; F_G, gravity; F_I, interaction force; F_F, friction force; HPMC, hydroxy propyl methyl cellulose; HPLC, high performance liquid chromatography; LAC, lactose carrier; MMSH, modular modified Sympatec HELOs; MSS, micronized salbutamol sulfate; MOC, micro orifice collector; MMAD, mass median aerodynamic diameter; MFV, minimum fluidization velocity; NGI, Next Generation Impactor; O, oxygen; PDP, pulmonary delivery process; *R*, release amount; R_{max}, maximum of release amount; R_{AUC}, total release amount; SEM, scanning electron microscope; *S*, stopping distance; T_{max}, the time to R_{max}; T_t, terminal time; U_0, air flow rate; V_0, velocity.

*Corresponding authors. Tel./fax: +86 20 39943115.
E-mail addresses: huangy2007@163.com (Ying Huang), panxin2@mail.sysu.edu.cn (Xin Pan).
†These authors made equal contributions to this work.

Peer review under responsibility of Institute of Materia Medica, Chinese Academy of Medical Sciences and Chinese Pharmaceutical Association.

https://doi.org/10.1016/j.apsb.2020.02.013

Real-time monitoring;
Modular modification;
Carrier;
Air flow rate;
Mechanism of drug delivery

(MMSH) was developed to fully investigate the mechanism of each PDP separately in real-time. An inhaler device, artificial throat and pre-separator were separately integrated with a Sympatec HELOS. The dispersion and fluidization, transportation, detachment and deposition processes of pulmonary delivery for model DPIs were explored under different flow rates. Moreover, time-sliced measurements were used to monitor the PDPs in real-time. The Next Generation Impactor (NGI) was applied to determine the aerosolization performance of the model DPIs. The release profiles of the drug particles, drug aggregations and carriers were obtained by MMSH in real-time. Each PDP of the DPIs was analyzed in detail. Moreover, a positive correlation was established between the total release amount of drug particles and the fine particle fraction (FPF) values ($R^2 = 0.9898$). The innovative MMSH was successfully developed and was capable of illustrating the PDPs and the mechanism of carrier-based DPIs, providing a theoretical basis for the design and optimization of carrier-based DPIs.

1. Introduction

Dry powder inhalations (DPIs) had attracted enormous attention worldwide by virtue of local targeting, rapid drug action, suitability for delivering a wide range of drugs and satisfactory patient compliance[1]. As a form of pulmonary drug delivery, DPIs had been widely applied in the treatment of pulmonary diseases, such as asthma[2], chronic obstructive pulmonary disease[3], pulmonary infections[4] and pulmonary cancer[5], as well as systematic diseases, such as diabetes[6] and schizophrenia[7]. In general, there were two types of DPIs, carrier-based DPIs and carrier-free DPIs. To achieve desirable pulmonary delivery efficiency, the active pharmaceutical ingredients (APIs) required micronization to achieve an aerodynamic diameter (d_{ae}) of 0.5−5 μm[8]. However, the micronized APIs were prone to be cohesive, resulting in deterioration of flowability and dispersibility[9]. Thus, coarse carriers in the range of 50−200 μm[8] were frequently used to promote the flowability, dispersibility, blend homogeneity of DPIs and reduce the cohesion of micronized APIs[9]. According to a large number of studies, carriers played an important role in the manufacture and usage of DPIs[10−13].

The pulmonary delivery processes (PDPs) of carrier-based DPIs were proposed based on years of the researches on pulmonary drug delivery system, which could be divided into the following four processes (Fig. 1): fluidization and dispersion of DPIs, transportation of the API–carrier complex, detachment of APIs from the carriers, and deposition of APIs in the lungs[11]. When DPIs was inhaled, air flow provided the initial kinetic energy, leading to the critical fluidization and dispersion of the DPIs. Subsequently, the DPIs was transported by air flow entrainment and passed through the oropharynx. Next, vortex air flow[14] in the bronchi bifurcation caused the APIs to detach from the carriers. Finally, the APIs were transported into the lower parts of the airways and deposited on the deep lung while the carriers were captured by the bronchi and cleared by cilia movement. It was commonly held that pulmonary drug delivery efficiency was mainly influenced by the transportation and detachment processes[12,15]. These two key processes were closely related to various factors, including the powder properties of the carrier[13,16,17], the interaction of API–carrier[18], and the content of fine particles[19,20]. In addition, the air flow pattern[21−23] produced by the inhaler device and the inhalation mode of patients, such as the

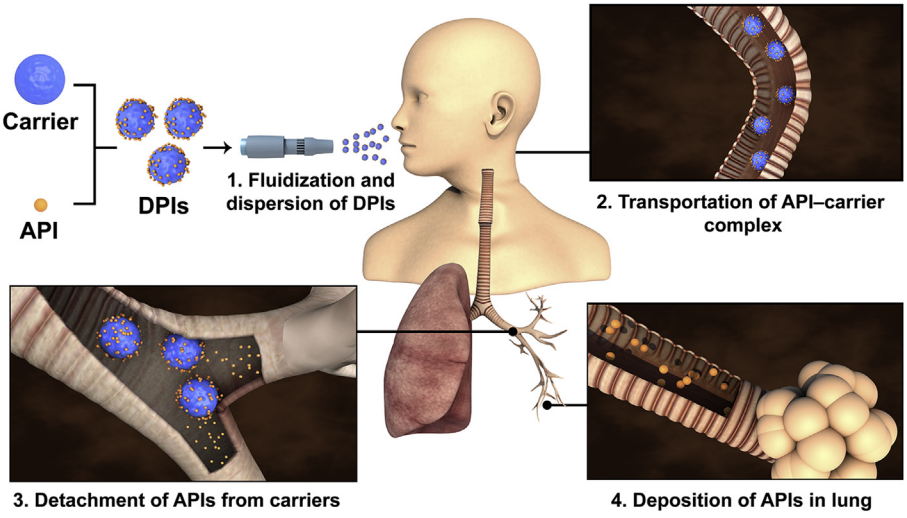

Figure 1 Schematic illustration of the pulmonary delivery process in carrier-based DPIs.

air flow rate[24,25] and duration of inhalation[26], also exerted a significant influence on the PDPs. In recent years, specific attention had been paid to collect evidence on the mechanism of PDPs. Elucidation of this issue could help to bridge the gap between formulation and pulmonary drug delivery efficiency of DPIs. Studies by means of cascade impactors and the computational fluid dynamics-discrete element method (CFD-DEM) had been the most frequent approaches in this field.

Cascade impactors, such as the Next Generation Impactor (NGI, Copley Scientific Ltd., Nottingham, UK) and Anderson Cascade Impactor (ACI, Copley Scientific Ltd.), had been the most common tools for the evaluation of DPIs, which were widely accepted by regulatory authorities including the *United States Pharmacopeia*, *European Pharmacopoeia* and *Chinese Pharmacopoeia*[27–29]. The drug deposition profile of DPIs could be acquired by cascade impactor analysis (CIA). Based on the above profile, the fine particle fraction (FPF) could be computed, which was a widely recognized indicator for the aerosolization performance of DPIs[30]. However, cascade impactor experiments were time-consuming and laborious due to complicated experimental operations and the subsequent quantification of APIs, which normally took several days or even weeks. In addition, limited information could be provided by CIA to explore the PDPs of DPIs, which were the prerequisite for DPIs formulation design and optimization. Therefore, the process to achieve the optimal formulation of DPIs *via* CIA was slow, without a clear improvement direction.

The CFD-DEM was supposed to be a powerful and functional tool to investigate the PDPs of DPIs[31]. Specifically, CFD could simulate the gas–solid hydrodynamics[32], and DEM was one of the most accepted methods for simulating the interactions of particle−particle/wall[33]. Thus, the simulation of air flow movement and particles in an inhaler device/throat/bronchi 3D model could be achieved by CFD-DEM, which had been broadly applied in DPIs over the past years. Generally, the applications of CFD-DEM had mainly focused on the design of inhaler devices[22,30] and dispersion mechanisms of DPIs actuated by air flow[34] and artificial throats[23,35]. However, the simplified and idealized models established by CFD-DEM impeded the further development of this type of modeling for DPIs because the actual and specific powder properties of DPIs were random and uncertain. For example, the surface morphology and the shape of the particles were complex, and the particle size was not uniform. The model of CFD-DEM neglected the individual differences of particles in actual on the overall process. Besides, the current researches of the CFD-DEM were mainly focused on a part of PDPs instead of the whole processes, which was attributed to the time-consuming and costly CFD-DEM model development covering inhaler device, throat and tracheal bronchus. In addition, the variable and heterogeneous air flow in humans was hard to achieve in CFD-DEM. Notably, the abovementioned factors were ubiquitous and had a great impact on the PDDs of DPIs, and thus, these parameters should not be neglected.

Sympatec HELOS laser diffraction (Sympatec GmbH, Clausthal-Zellerfeld, Germany) was a widespread particle size detection method used in the pharmaceutical[36,37], material[38,39], food[40] and even 3D printing industries[41]. An inhaler adapter (INHALER™, Sympatec GmbH, Clausthal-Zellerfeld, Germany) was specially designed to interface with Sympatec HELOS, aiming at detecting the particle sizes of DPIs. The system was composed of a device adapter, bent glass tube and pre-separator (Fig. 2). The device adapter had an exchangeable seal ring for the various shapes of mouthpieces that could comply with different demands of inhalation devices. The bent glass tube served as an artificial throat, and the pre-separator mimicked the bronchi bifurcation. Because INHALER™ resembled the human respiratory tract structure, the particle size obtained was close to the d_{ae}[42]. However, the standard configuration and test of Sympatec HELOS & INHALER™ only offered a final mean particle size distribution, which did not provide sufficient information for investigations of PDPs.

To obtain the detailed PDPs of DPIs, the following factors should be fully taken into consideration. The PDPs of carrier-based DPIs in inhaler device, throat and bronchi needed to be explored separately in real-time to understand the effect of each part on the efficiency of pulmonary drug delivery. In addition, the real particle size, surface morphology and electrical properties of the particles should be considered. In light of the complex interdependencies of the above factors, it was of great scientific and industrial importance to systematically develop a new and feasible approach to elucidate PDPs, laying a firm basis for enhancing the efficiency of the design and optimization of DPIs.

In the present study, a modular modified Sympatec HELOS (MMSH) was first developed for probing the mechanisms of the PDPs of DPIs. An inhaler device, artificial throat and pre-separator were creatively separately integrated with a Sympatec HELOS. The inhaler device was employed to investigate the dispersion and fluidization processes of DPIs. An artificial throat was used to simulate the direction changes of air flow, and a pre-separator was applied to mimic bronchi bifurcation, where the

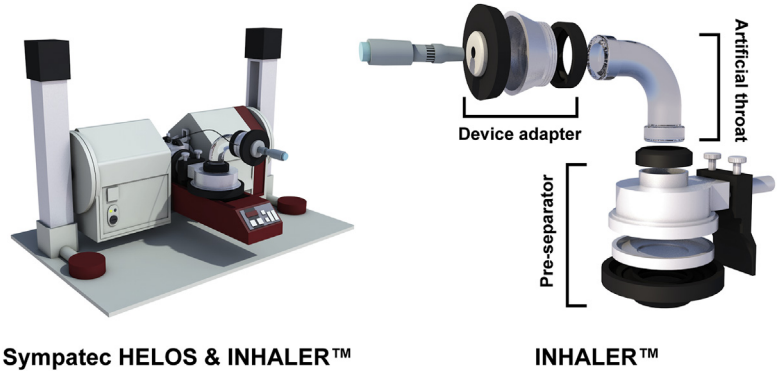

Figure 2 Schematic diagram of Sympatec HELOS & INHALER™.

transportation and detachment processes occurred. The established MMSH method was generally suited for various formulations, and competent for different inhaler devices with corresponding adapters. Additionally, time-sliced measurement was firstly applied for real-time monitoring of the release profiles of the drug particles, carriers and DPIs, where the contribution of individual particles would be reflected.

The MMSH test was fast and could be performed in 1 min. The mechanism of DPIs PDPs was elaborated in detail. In addition, the impact of air flow rates (U_0) on the PDPs of DPIs was identified based on the MMSH. Moreover, the NGI was employed to determine the aerosolization performance of DPIs. A desirable positive correlation between the results of MMSH and NGI was established, suggesting that the MMSH was a time-saving and credible alternative for efficient design and optimization of DPIs.

2. Materials and methods

2.1. Materials

Respitose® SV003 lactose was generously donated by DFE Pharma (Goch, Germany). Salbutamol sulfate was purchased from Bidepharmatech Co., Ltd. (Shanghai, China). 3# Hydroxy propyl methyl cellulose (HPMC) capsule (Vcaps®) was provided by Capsugel Co., Ltd. (Suzhou, China). Methanol (analytically pure grade) was supplied by Honeywell Burdick & Jackson Inc. (Morris, NJ, USA). Acetonitrile (analytically pure grade) was obtained from Saen Chemical Technology Co., Ltd. (Shanghai, China). Monopotassium phosphate was purchased from Damao Chemical Reagent Factory (Tianjin, China).

2.2. Preparation of model DPIs

2.2.1. Micronization of salbutamol sulfate

Salbutamol sulfate was selected as the model drug in the present study. Micronized salbutamol sulfate (MSS) was obtained by jet-mill (J-20, TECNOLOGIA MECCANICA, Torino, Italy) with 6 kPa ring pressure and 7 kPa Venturi pressure. The particle size of MSS was determined subsequently.

2.2.2. Sieving of lactose carrier

Respitose® SV003 was the inhalation grade lactose and commonly used as DPIs carrier[43,44]. On account of the wide span of particle size in Respitose® SV003 (D_{10} = 19−43 μm, D_{50} = 53−66 μm , D_{90} = 75−106 μm), sieving method was employed to narrow the span for further study. Respitose® SV003 was sieved through the sieve of 125 and 75 μm for 20 min by a vibratory sieving (AS200, RETSCH, Haan, Germany). Lactose carrier (LAC) was obtained by collecting the fraction of Respitose® SV003 between two sieves.

2.2.3. Particle size distribution

The particle size of MSS and LAC was analyzed by laser diffraction particle size analyzers including Malvern Mastersizer 2000 (Malvern Instruments Ltd., Malvern, Worcestershire, UK) and Sympatec HELOS & INHALER™. The samples were dispersed by the Scirocco 2000 dry powder feeder apparatus under a pressure of 3.5 bar prior to the tests of Malvern Mastersizer 2000. In regard to Sympatec HELOS & INHALER™, the single dose inhaler Turbospin® (PH&T S.p.A., Milan, Italy) was integrated with the INHALER™ for dispersion. The measurements were conducted under the U_0 of 60 L/min with the 0.5% optical concentration (C_{opt}) for trigger, and ended with the C_{opt} less than 0.5%. Moreover, R2 lens with a measurable particle size range of 0.25/0.45−87.5 μm and R4 lens with a measurable particle size range of 0.5/1.8−350 μm were selected to evaluate the particle size of MSS and LAC, respectively. Particle size was calculated by Fraunhofer theory in WINDOX 5.0 software (Sympatec GmbH). Each sample was quantified in triplicate.

2.2.4. Preparation and homogeneity test of model DPIs

The model DPIs was produced by blending MSS and LAC at a ratio of 1:15 (*w*/*w*), using a Turbula T2F mixer (Glen Creston Ltd., Middlesex, UK) at 46 rpm for 60 min[20]. The obtained model DPIs was packed into 3# Vcaps® capsules (Capsugel Co., Ltd.) with 10 ± 0.5 mg. After blending, the homogeneity of drug content in DPIs was assessed. Ten random capsules were taken and dissolved in 10 mL of ultrapure water, and the content of MSS was then quantified by high performance liquid chromatography (HPLC).

2.2.5. High performance liquid chromatography

The content of MSS was quantified by HPLC (LC-20, Shimadzu Co., Ltd., Kyoto, Japan) with a UV-detector at 276 nm. C18 column (250 mm × 4.6 mm, 5 μm, OSAKA SODA Co., Ltd., Osaka, Japan) was used and the column temperature was set as 35 °C. The mobile phase was 0.13% monopotassium phosphate (adjusted to pH 3 with phosphoric acid):methanol = 85:15 (*v*/*v*) at a flow rate of 1 mL/min.

The content of LAC was quantified by HPLC with an evaporative light-scattering detector (ELSD-LT II, Shimadzu Co., Ltd.), using an NH_2 column (250 mm × 4.6 mm, 5 μm, OSAKA SODA Co., Ltd.). The column temperature was 35 °C and the mobile phase was acetonitrile:ultrapure water = 70:30 at a flow rate of 1 mL/min. The temperature of the drift tube was set at 50 °C and gas pressure was 350 kPa. Each sample was quantified in triplicate.

2.3. Scanning electron microscopy and energy-dispersive X-ray spectroscopy

Gemini 500 scanning electron microscope (SEM, Bruker, Ettlingen, Germany) equipped with energy-dispersive X-ray spectroscopy (EDXS) was adopted to characterize the morphology and chemical element distribution on the surface of particles. Sample powder was placed on aluminum stubs prior to imaging. The SEM and EDXS images were captured at an acceleration voltage of 2.0 and 5.0 kV, respectively. Oxygen and sulfur spectra were captured by EDXS, which represented LAC ($C_{12}H_{22}O_{11}$) and MSS [$(C_{13}H_{21}NO_3)_2 \cdot H_2SO_4$], respectively.

2.4. Pulmonary delivery processes investigation of DPIs by MMSH

MMSH was used to investigate the mechanism of PDPs in DPIs. The instrument configuration was depicted in Fig. 3A. Three different configurations were set up by the authors in order to explore the impact of the inhaler device (Fig. 3B), the artificial throat (Fig. 3C) and the pre-separator (Fig. 3D) on the PDPs under different U_0. The single dose Turbospin® was served as the model

inhaler device. The measurements were conducted under the U_0 of 30, 60 and 80 L/min, respectively, with the following parameters. Start and stop of the measurements was triggered on a C_{opt} of 1.0% and 0.5%, respectively, with a R4 lens. The data were recorded in 100 ms sections with a 25 ms time base. The measurement duration was 4 s. Each sample was quantified in triplicate. WINDOX 5.0 software was employed to analyze the data. The obtained data were analyzed and the involved parameters were descripted in Table 1[48]. The product of C_{opt} and dQ_3 was defined as release amount of particles (R), which was recorded in each 100 ms. Release profile was plotted by time (T) as X-axis and R as Y-axis and connected with smooth curve. The area under the curve of release profile was defined as R_{AUC}, which was deduced by integration method of Origin 8.5 Software (Origin Lab, Northampton, MA, USA).

Table 1 Description of parameters.

Parameter	Description
C_{opt}	Optical concentration
dQ_3	The volume percentage of particles within certain range $dQ_3 = Q_3(D_{i1}) - Q_3(D_{i2})$ Q_3 represented volume cumulative distribution D_i represented the particle size $(D_{i1} > D_{i2})$ $Q_3(D_i) =$ Total volume of particles that smaller than D_i/Total volume of particles
R	Release amount, $R = C_{opt} \times dQ_3$
R_{max}	Maximum of release amount
T_{max}	The time of R_{max}
T_t	Terminal time, the time corresponding to the last R
R_{AUC}	Total release amount, the area under the curve of the release profile

2.5. *In vitro aerosolization performance investigation of DPIs by NGI*

The *in vitro* aerosolization performance of model DPIs was detected by the NGI with or without a pre-separator, according to the standard of *European Pharmacopoeia* 8.0. The single dose inhaler Turbospin® was used to connect with the NGI. The surface of particle collection plate of each stage was coated with Tween® 80 (1% in ethanol, *v*/*v*) prior to test to prevent inter-stage losses due to the particle bounce. A batch of 30 capsules was shot in each run (4 kPa pressure drop) with different U_0 and time, namely 30 L/min–8 s, 60 L/min–4 s and 80 L/min–3 s. Subsequently, MSS and LAC retained on the inhaler and deposited in the adaptor, induction port, pre-separator, all NGI stages and MOC were rinsed with ultra-pure water. The deposition profiles of MSS and LAC were obtained by HPLC quantification. Three replicates were carried out for each U_0. The FPF, fine particle dose (FPD), emitted dose (ED) and mass median aerodynamic diameter (MMAD) values were calculated by CITDAS® software (version 3.10, Copley Scientific Ltd.).

2.6. *Statistical analysis*

All the data were presented as mean ± SD, if possible. SPSS Statistics V 17.0 software (IBM Co., Armonk, NY, USA) was applied for statistical analysis. One-way analysis of variance (ANOVA) and unpaired two-sample t test were employed to the experimental data above, where $P < 0.05$ was considered to be

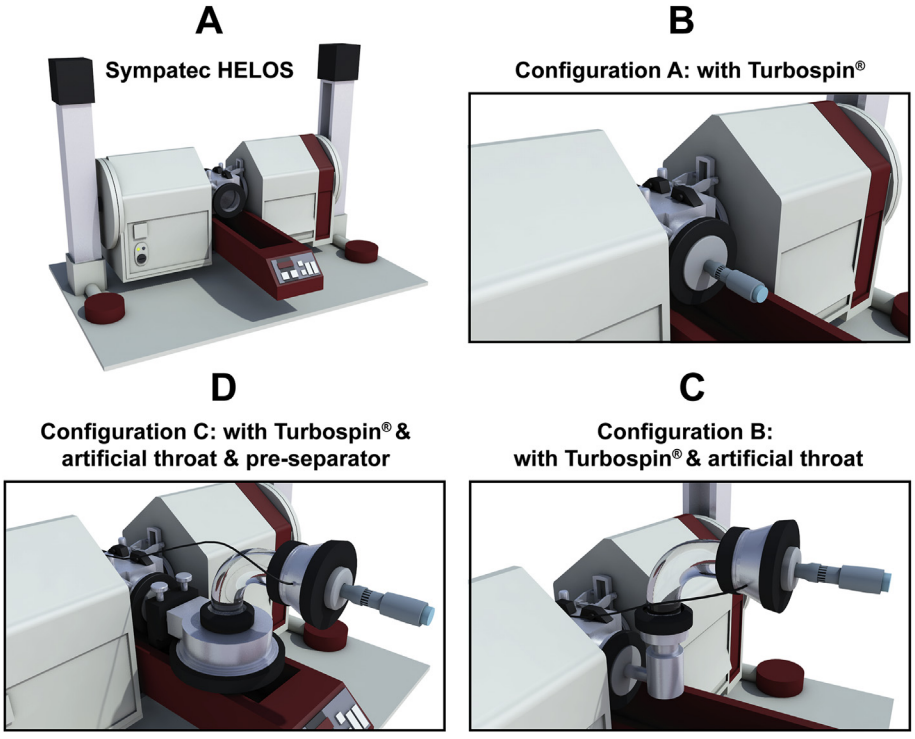

Figure 3 Schematic diagram of instrument conuration (A) Sympatec HELOS; (B) Conuration A: Sympatec HELOS with Turbospin®; (C) Conuration B: Sympatec HELOS with Turbospin® & artificial throat; (D) Conuration C: Sympatec HELOS with Turbospin® & artificial throat & pre-separator.

statistically significant, and an R^2 value higher than 0.9 suggested a strong correlation.

3. Results and discussion

3.1. Particle size distribution and homogeneity

Particle size distribution and relevant parameters of MSS and LAC were presented in Table 2. D_{50} values of MSS obtained by two instruments were both smaller than 5 μm, suggesting it was potential for pulmonary drug delivery. Besides, D_{50} values of LAC were much larger than MSS. Particle size distributions of MSS and LAC were not overlap and presented normal distribution (Supporting Information Fig. S1). It meant that MSS and LAC could be distinguished by laser diffraction and were applicable in the investigation of PDPs in DPIs. For homogeneity test, the average recovery of MSS was 101.58 ± 0.93%, suggesting a desirable homogeneity in DPIs.

Compared with Sympatec HELOS & INHALER™, particle size obtained from Malvern Mastersizer 2000 was smaller. DPIs was compulsively dispersed by the steel balls of Scirocco 2000 dry powder feeder in Malvern Mastersizer 2000[11]. Thus, particle size determined by Malvern Mastersizer 2000 was the geometry size of particles. On the contrary, Sympatec HELOS & INHALER™ simulated the impaction and deposition of DPIs in the real inhalation process. Therefore, the obtained particle sizes were closer to the d_{ae}, which was defined as the inherent tendency of gravitational settling or inertial impaction caused aerosol deposition. In addition, Sympatec HELOS & INHALER™ did not forcibly dispersed DPIs and thus the obtained particle sizes were larger than that of Malvern Mastersizer 2000. Therefore, Sympatec HELOS INHALER™ was more suitable for evaluation of particle size distribution of DPIs[45,46].

The particle sizes obtained from Sympatec HELOS & INHALER™ were served as the references for the drug and carrier. Specifically, D_{10}–D_{90} of MSS and LAC were defined as the size of primary drug and carrier, and the fraction between D_{90} of MSS and D_{10} of LAC was defined as drug aggregation. The detail was as follow: drug: 1.13−6.81 μm; carrier: 43.63−118.25 μm; drug agglomeration: 6.81−43.63 μm.

3.2. Scanning electron microscopy and energy-dispersive X-ray spectroscopy

The morphology of MSS, LAC and model DPIs was shown in Fig. 4A–C. MSS was strip shape with uniform size (Fig. 4A). LAC was tomahawk shape with flat surface and was covered by some fine lactose (Fig. 4B). After blending, strip shape MSS evenly distributed on the surface of LAC in the DPIs (Fig. 4C). Fig. 4D, F and H were the optical images of lactose (LAC), micronized salbutamol sulfate (MSS) and DPIs in the EDXS, respectively. Based on this, the oxygen spectra (yellow color) of LAC (Fig. 4E) and sulfur spectra (purple color) of MSS (Fig. 4G) were captured by EDXS for further distinction MSS from LAC in the DPIs. Hence, the oxygen spectra (Fig. 4I), sulfur spectra (Fig. 4J) and merged image (Fig. 4K) of DPIs suggested most of the MSS was evenly distributed on the surface of LAC while a small number of MSS aggregation existed.

3.3. Pulmonary delivery processes investigation of DPIs by MMSH

The PDPs played a key role in the formulation design and optimization of the DPIs. Generally, the inhaler device, artificial throat and pre-separator contributed to different levels of transportation and detachment because of their physical structures. Therefore, the MMSH was applied to explore the impacts of these parameters separately on the mechanisms of the dispersion, fluidization, transportation, detachment and deposition processes of DPIs. Additionally, the impact of flow rate (U_0) on the PDPs of DPIs was investigated.

3.3.1. Configuration A: with Turbospin®

First, the inhaler device Turbospin® was integrated with the Sympatec HELOS to probe the fluidization and dispersion processes of DPIs and their early deposition in the inhaler device. The release (R) of the carriers, drug aggregations and drug particles could be monitored in real time, revealing the inhalation mode of DPIs. Additionally, R_{AUC} was obtained by integrating the release profile, which indicated the detachment and deposition of DPIs.

The release profile of the DPIs was depicted in Fig. 5A. The R values of the DPIs presented the same tendencies of first increasing and then decreasing at different U_0. With increasing U_0, R_{max} increased while T_t decreased. Specifically, the DPIs at 60 and 80 L/min showed 2- and 2.4-fold increase in R_{max} compared with the R_{max} at 30 L/min, respectively. In addition, a good linear relationship ($R^2 = 0.9887$) was established between R_{max} and U_0 (Fig. 5A). Regarding the R_{AUC} of the DPIs (Fig. 5E), when U_0 increased from 30 to 60 L/min, R_{AUC} increased 1.51-fold. It was worth noting that there was no significant difference between the R_{AUC} at 60 L/min and that at 80 L/min ($P > 0.05$).

When DPIs particles released from the capsule, the particles were subjected to many forces, including drag force from air flow (F_D)[47,48], gravity force (F_G)[49], interaction force between particles (F_I)[50,51] and friction force (F_F) between the particles and capsule wall[52] (Fig. 5F). At low U_0, the F_D [Eq. (1)][53] acting on the DPIs particles was too small to overcome the F_I and/or F_F.

$$F_D = 3\pi\eta X d U_0 / C_C \quad (1)$$

where η represents the viscosity of the air, X denotes the dynamic shape factor, d represents the diameter of the particle and C_C is the Cunningham correction factor for slip flow.

Therefore, the DPIs particles were prone to remain in the capsule or deposit prematurely without reaching the detector due

Table 2 Particle size distribution of MSS and LAC (the data were presented as mean ± SD, $n = 3$).

Instrument	Formu-lation	D_{10} (μm)	D_{50} (μm)	D_{90} (μm)	Span
Malvern Mastersizer 2000	MSS	0.70 ± 0.03	2.01 ± 0.15	4.66 ± 0.31	2.67 ± 0.03
	LAC	33.35 ± 0.79	74.25 ± 0.52	109.12 ± 0.66	1.92 ± 0.01
Sympatec HELOS &INHALER™	MSS	1.13 ± 0.07	2.74 ± 0.03	6.81 ± 0.22	2.90 ± 0.07
	LAC	43.63 ± 0.92	83.90 ± 0.54	118.25 ± 1.39	1.93 ± 0.02

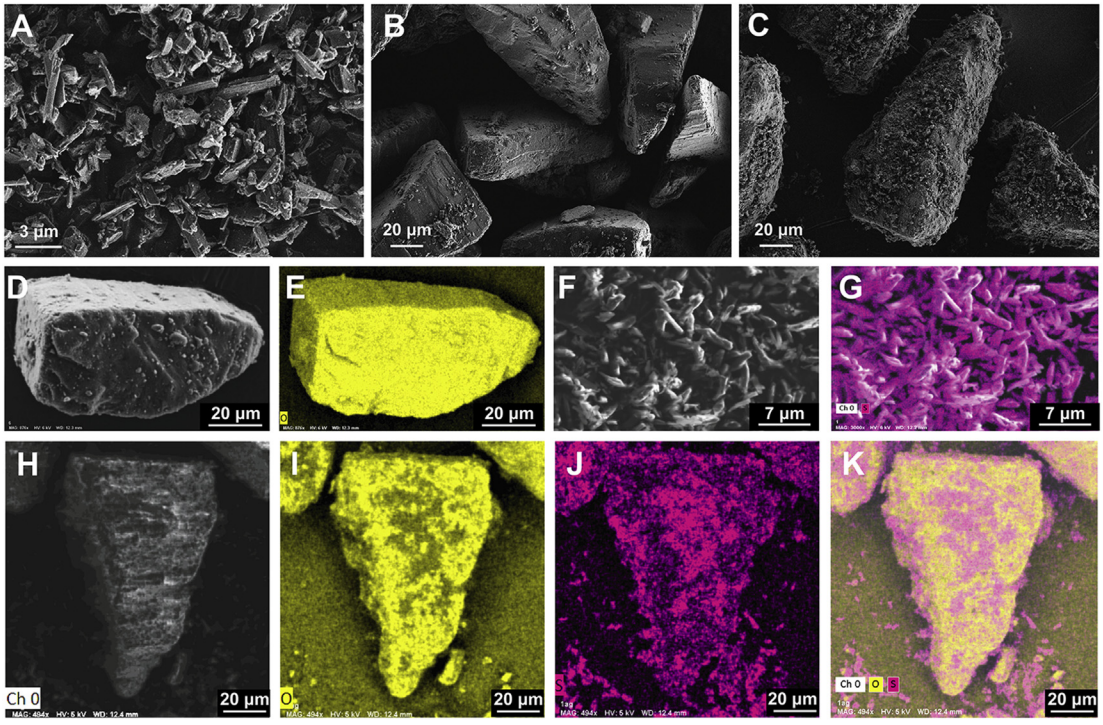

Figure 4 SEM images of (A) MSS; (B) LAC; (C) DPIs; EDXS images of (D) LAC optical image; (E) LAC oxygen spectra; (F) MSS optical image; (G) MSS sulfur spectra; (H) DPIs optical image; (I) DPIs oxygen spectra; (J) DPIs sulfur spectra; (K) DPIs merged image. MSS, micronized salbutamol sulfate; LAC, lactose carrier; DPIs, dry powder inhalations; EDXS, energy-dispersive X-ray spectroscopy.

to the counteracting of F_D (Fig. 5G). Notably, the particles on the surface of the powder bed encountered a smaller F_I and were easily entrained by air flow and release. Thus, the powder bed of DPIs in the capsule was gradually and slowly eroded from the surface until the release was complete (Fig. 5H). Therefore, the R_{AUC} and R_{max} were low at 30 L/min, while T_t was long. These results suggested that low inhalation U_0 generated a gradual inhalation process, resulting in an early deposition of DPIs in the oropharynx instead of delivering to the lower airways.

In contrast, the pressure difference between the inside and outside of the capsule increased with increasing U_0. A higher U_0 supplied a larger F_D to the DPIs, rendering the particles sufficient initial kinetic energy to overcome F_I and F_F; thus, the fluidization of DPIs could be achieved. Moreover, the acceleration (a) of the particle increased with increasing U_0 [Eq. (2)][54].

$$a = F_D/m = F_D/\rho V = 6F_D/\rho\pi d^3 = 18\eta X U_0/C_C\rho d^2 \quad (2)$$

where ρ represents the bulk density, X denotes the dynamic shape factor, d represents the diameter of the particle, C_C is the Cunningham correction factor for slip flow, m represents the mass of the particle and V is the volume of the particle.

The accelerated movement of DPIs particles led to bursting inhalation and the release of high-density aerosol clouds at short notice (Fig. 5I). Hence, R_{max} increased and T_t shortened with increasing U_0. Furthermore, a larger F_D enabled the particles to be entrained by the air flow rather than prematurely depositing, which contributed to the increase in R_{AUC}. Thus, bursting inhalation was more easily formed by higher U_0, which was beneficial to achieve higher R_{AUC} and efficient pulmonary drug delivery. The result was also in accordance with some similar CFD-DEM studies. The dispersion number of API particles detached from the carrier increased with increasing air velocity[34] and the deposition of DPIs on the inhaler device was decreased with increased air flow[55].

In addition, there were no significant differences ($P > 0.05$) in R_{AUC} between 60 and 80 L/min, indicating that 60 L/min satisfied the minimum fluidization velocity (MFV) of DPIs particles. In addition, the release profile of the carriers was similar to that of the DPIs since the detachment of carrier–drug/drug aggregation was weak in the fluidization and dispersion processes.

In regard to the drug particles and drug aggregations, R_{max} increased and T_t decreased with increasing U_0 (Fig. 5B–C). The R_{max} of drug particles at 60 and 80 L/min markedly increased to 3.3- and 5.8-fold of 30 L/min, respectively. A satisfactory linear relationship between the R_{max} of drug particles and U_0 was demonstrated ($R^2 = 0.9817$). In addition, when U_0 increased to 80 L/min, the R_{max} of drug aggregations was 2-fold of 30 L/min. The R_{AUC} of drug particles increased by 3.9-fold with the increment of U_0 from 30 to 80 L/min, while the R_{AUC} of drug aggregations showed no distinct change ($P > 0.05$).

The Turbospin® possessed high grid voidage, which easily yielded turbulence during inhalation[22]. The intensity of the turbulence was affected by U_0[21]. At low U_0, the turbulence intensity was weak and induced slow fluidization of DPIs particles. In this gradual inhalation process, the particles collided with each other slowly and gently in the turbulence, and thus, the drug particles and drug aggregations were gradually detached from the carriers, which was responsible for the long T_t and low R_{max}. In contrast, the turbulence became stronger at higher U_0. The high R_{max} and short T_t indicated burst inhalation of DPIs, which resulted in high-density aerosol clouds. These conditions rendered a greater chance of collision and were conductive to the detachment process. Consequently, the drug

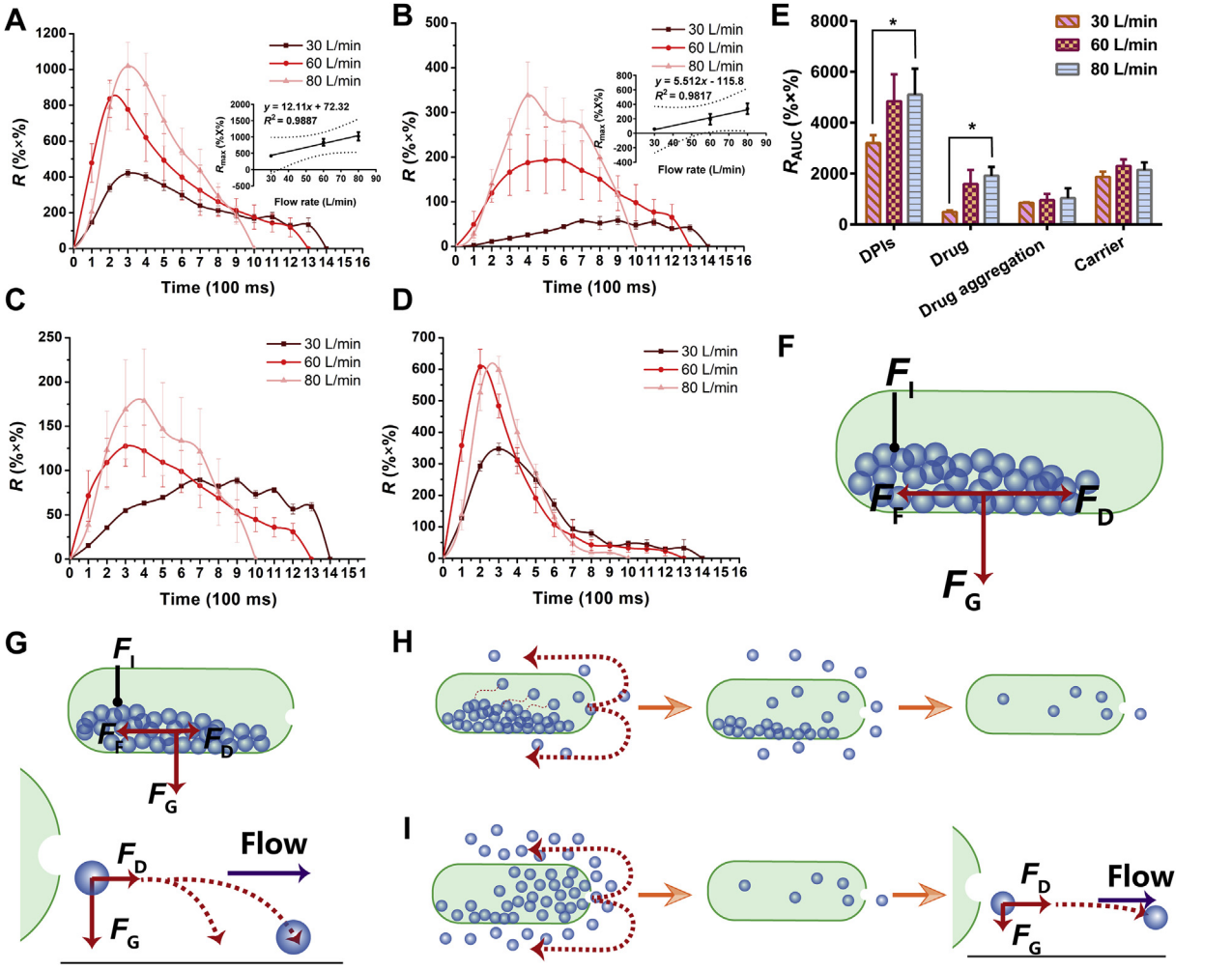

Figure 5 Release profiles and total release amount of conuration A. (A) Release profiles of DPIs. Inset was the correlation between U_0 and R_{max}; (B) Release profiles of Drug. Inset was the correlation between U_0 and R_{max}; (C) Release profiles of drug aggregation; (D) Release profiles of carrier; (E) Total release amount at different flow rates; (F) Force analysis of DPIs in the capsule; (G) DPIs remained in the capsule or deposited prematurely; (H) The release of DPIs from capsule at low U_0; (I) The release of DPIs from capsule at high U_0 (All the data were presented as mean ± SD, $^*P < 0.05$, $n = 3$).

particles were released instantly, and the R_{AUC} of drug particles increased. Nevertheless, the R_{AUC} of drug aggregations showed no obvious difference ($P > 0.05$), suggesting that the drug−drug particles interaction forces (*e.g.*, Coulomb force, capillary force, and van der Waals force[51]) were larger than those of drug−carrier and the force of collision was not large enough to overcome these forces.

In summary, the fluidization and dispersion processes of DPIs could be monitored individually by configuration A. According to the real-time release profile, the DPIs was fluidized and released from the capsule when inhaled. The DPIs was dispersed due to the turbulence induced by the high voidage grid structure of the inhaler device. Some of the drug particles and drug aggregations detached from the carriers under turbulence by impaction with the wall of the inhaler device. In addition, the inspiratory U_0 had a great impact on the fluidization and dispersion processes. The inhalation mode of the DPIs under different U_0 could be deduced from the real-time release profiles. Gradual inhalation at low U_0 resulted in more early deposition that was not conducive to further delivery of DPIs. In contrast, bursting inhalation of DPIs occurred at high U_0, which caused more DPIs to be transported into deeper airways instead of depositing. Thus, stronger turbulence and bursting inhalation were favorable for detachment of drug−carrier in the inhaler device.

Some studies reported on the impact of inspiratory U_0 on the pulmonary drug delivery efficiency of DPIs, and the results were contradictory and inconclusive[56,57]. These variations were ascribed to the many complex factors associated with PDPs, such as the formulation, inhaler device and inspiratory flow rate[58]. The present study offered an approach for evaluating the relationship between inspiratory U_0 and the release profile of DPIs. Through the combination of the transportation and detachment processes in artificial throat and pre-separator, the optimal inspiratory U_0 as well as the inhalation mode with certain formulations and inhaler device could be acquired quickly.

3.3.2. *Configuration B: with Turbospin® & artificial throat*

The inhaler device Turbospin® and artificial throat were integrated with the Sympatec HELOS through a customized connector to investigate the effect of the throat on the transportation and detachment mechanism of DPIs during inhalation.

The release profile of configuration B was shown in Fig. 6A–D. Compared with the release profile of configuration A (Fig. 5A–D), the R_{max} and R_{AUC} of the DPIs decreased sharply at each U_0, which might be due to the following two reasons. First, when the DPIs particles were released from the inhaler device and reached the artificial throat, the particles were subjected to F_D and F_G. The DPIs deposited before the bend in the artificial throat due to insufficient F_D (Fig. 6F). In addition, the bend in the artificial throat changed the direction of air flow, while the particles still possessed a velocity (V_0) in the original direction[53]. On account of the inertia of the particles, the particles kept moving in the original direction[59]. The distance needed to reduce V_0 to zero by the action of the resistance force was defined as the stopping distance [S, Eq. (3)][53].

$$S = d^2 \rho U_0 C_C / 18 \eta X \quad (3)$$

where η represents the viscosity of the air, X denotes the dynamic shape factor, d represents the diameter of particle, ρ represents the bulk density and C_C is the Cunningham correction factor for slip flow.

When S was longer than the distance between the particle and the wall of the throat, there was a greater chance for the particle to impact the wall and be captured. Thus, the number of particles that could successfully pass through the artificial throat markedly dropped.

Additionally, the R_{AUC} of drug particles decreased sharply at each U_0 after the addition of the artificial throat. It was worth noting that the detached drug particles were small size, which enabled the particles to deviate more from the center of the artificial throat than the large carriers and be easily captured by the throat[35]. In addition, fine drug particles easily generated electrostatic force[51], and thus, these particles tended to adhere to the throat wall. Therefore, the drug particles detached in the inhaler device or artificial throat were easy to be captured and hard to be transported to the lower parts of the airway, which was not desirable for pulmonary drug delivery.

It was well known that a real human throat possessed more complex internal geometry as well as mucus layers[60]. Once the DPIs particle impacted the wall of the throat, the particle had a high probability to be captured immediately without bouncing back. Thus, more throat deposition would exist in the human body. Alberta throat with more detailed internal geometry could be employed in the future to mimic the actual structure of human throats. In addition, the throat could be coated with a material, such as 1% Tween® 80[61], to simulate the mucus layer and acquire a higher correlation between *in vitro* and *in vivo* tests. With respect to the release profile of configuration B under different U_0 (Fig. 6A–D), R_{max} and R_{AUC} increased with increasing U_0. The R_{max} of the DPIs at 80 L/min was 1.63-fold and 3.02-fold of 60 and 30 L/min, respectively. With the addition of the artificial throat, the R_{max} of the DPIs and U_0 still had a good linear relationship ($R^2 = 0.9577$). According to the release profile (Fig. 6A), gradual inhalation (low R_{max} and long T_{max}) of the DPIs occurred at low U_0 when particles were slowly entrained by the air flow. Under this circumstance, inadequate F_D led to early deposition of DPIs. In contrast, high U_0 generated burst inhalation, and thus airborne particles moved faster because of larger F_D. More particles could be quickly fluidized (high R_{max} and short T_{max}). Although a higher U_0 induced a longer S and increased the deposition of DPIs at the throat, the R_{max} and R_{AUC} of the DPIs still increased. This result suggested that the increment of fluidized particles was higher than the decrease caused by deposition.

For the drug particles and drug aggregations (Fig. 6B and C), the R_{AUC} of drug at 30 L/min increased to 1.46- and 2.01-fold with increasing U_0, while the R_{AUC} of drug aggregations decreased. As mentioned above, the R_{AUC} of DPIs increased during bursting

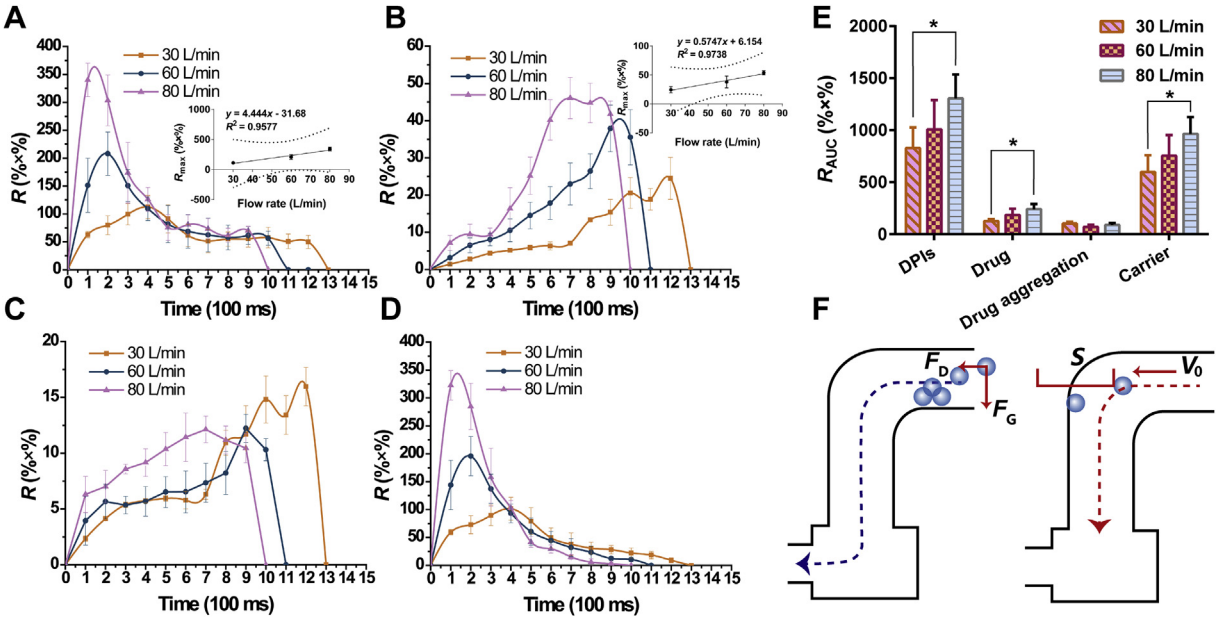

Figure 6 Release profiles and total release amount of conuration B. (A) Release profiles of DPIs. Inset was the correlation between U_0 and R_{max}; (B) Release profiles of drug. Inset was the correlation between U_0 and R_{max}; (C) Release profiles of drug aggregation; (D) Release profiles of carrier; (E) Total release amount at different flow rates; (F) DPIs deposited before the corner of artificial throat and the stopping distance of particle was longer than the distance between particle and the wall of throat (All the data were presented as mean ± SD, $^*P < 0.05$, $n = 3$). U_0, air flow rate; R_{max}, maximum of release amount.

inhalation, and thus the detachment of the drug due to impaction increased. Additionally, the R_{AUC} of drug aggregations decreased with increasing U_0. The drug aggregations more easily impacted the wall of the artificial throat due to the longer S at high U_0. The impaction force was capable of breaking a portion of the drug aggregations into fine drug particles. Therefore, the R_{AUC} of drug aggregations decreased while the R_{AUC} of drug particles increased.

In brief, the addition of an artificial throat mimicked the bend of the throat as well as the change in the air flow direction, which separately explored the transportation and detachment processes of DPIs in the throat. The R_{AUC} of DPIs sharply decreased compared with that of configuration A. A fraction of the released DPIs deposited before the bend of throat and part of the DPIs impacted the wall of the artificial throat due to the inertia of particles, hindering the further transportation of the DPIs to some extent. Additionally, the number of drug particles detached from the carriers in the inhaler device markedly dropped since these particles possessed a great chance to be captured by the throat owing to their electrostatic forces and movement locus close to the throat wall. The impaction force between the DPIs and the wall of the throat overcame the adhesive force between the carrier–drug/drug aggregation and promoted detachment and disaggregation in the throat, which was undesirable for its further transportation into deeper airways.

The release profile of configuration B also confirmed the higher R_{AUC} of DPIs as well as the higher R_{AUC} of drug particles in bursting inhalation rather than gradual inhalation. With the increment of U_0, more drug particles detached from the carriers due to a larger F_D and impaction in stronger turbulence. Nevertheless, the drug detached before or within the throat was easily deposited on the throat. Thus, further transportation and detachment of DPIs in pre-separator was needed for a thorough investigation.

3.3.3. *Configuration C: with Turbospin® & artificial throat & pre-separator*

The inhaler device Turbospin®, artificial throat and pre-separator were integrated with the Sympatec HELOS. A pre-separator mimicking the detached function of bronchi bifurcation was used to explore the detachment process of DPIs. The release profile of configuration C was shown in Fig. 7A–D. In contrast to the release profile of configuration B (Fig. 6A–D), R_{max} and R_{AUC} of DPIs rose dramatically, which mainly resulted from the increase in R_{max} and R_{AUC} of drug particles and drug aggregations. When DPIs particles entered the pre-separator, they moved by the entrainment of vortex air flow. The particles were subjected to centrifuge forces (F_C), F_D and F_G. F_C was proportional to the third power of the particle diameter [Eq. (4)][53].

$$F_C = mU_0^2/r = \pi d^3 U_0^2/6r \quad (4)$$

where m represents the mass of particle, r denotes the radius of centrifugal motion, d represents the diameter of particle.

Thus, the diameter of the particles had a great influence on the magnitude of F_C. The diameter of the carriers was much larger than those of the drug aggregations and drug particles. Hence, the larger F_C on the carriers expedited their movement locus to close to the wall of the pre-separator. In contrast, the drug aggregations and drug particles were inclined to move near the pre-separator center due to smaller F_C (Fig. 7F). The difference in F_C was greater than the adhesive force between the carriers and drug aggregations/drug, which facilitated considerable detachment. Therefore, the R_{max} and R_{AUC} of drug particles and drug aggregations increased sharply, indicating that pre-separator was efficient to detach carrier–drug owing to the vortex air flow. The drug particles detached at this stage and got a great chance to be transported into deeper airways and deposited in the lungs.

In addition, the R_{max} and R_{AUC} of carriers decreased compared with configuration B. The movement locus of the carriers was close to the pre-separator wall, which caused impaction and friction between the carriers and wall, resulting in the gradual loss of kinetic energy in the carriers. Moreover, as the particles moved with the vortex air flow, the particles also moved downward due to F_G. The carriers with larger masses were subjected to larger F_G than the drug aggregations and drug particles. Therefore, the carriers were more likely to deposit on the bottom of pre-separator without entering the detector, resulting in decreases in R_{max} and R_{AUC}. On the contrary, the smaller F_G prompted the drug aggregations and drug particles to be entrained by air flow and reach the detector. In the bronchi bifurcation of humans, the narrowing of bronchi led to an instant increase in the air flow rate. The F_C of vortex air flow in this area caused detachment of carrier–drug. The carriers were captured by the bronchi, while the drug particles were transported into the lower parts of the airways and deposited in the deep lungs. These processes were confirmed by the obtained results.In regard to the release profile at 30 L/min, the R of DPIs first increased and reached a plateau for a short time before declining, with no obvious peak (Fig. 7A). The release profile of drug aggregations and drug particles was similar to that of DPIs, which also presented gradual inhalation (Fig. 7B–C). However, the carriers could barely be detected at U_0 (Fig. 7D). At 30 L/min, the F_D acting on the DPIs particles was relatively small, and the particles were mainly subjected to F_G and quickly deposited on the bottom of pre-separator (Fig. 7G). Some of the drug particles and drug aggregations detached from the carriers before deposition. Most of the particles and aggregations were deposited with the carriers, which swirled with air flow at the bottom and the drug particles/drug aggregations impacted each other. The adhesive force between carrier–drug/drug aggregation was surmounted by the impaction force, causing slow and inefficient detachment (Fig. 7H). Additionally, the drug particles and drug aggregations were subjected to smaller F_G and larger F_D than the carriers, which enabled the particles and aggregations to be entrained by air flow again and to reach the detector. Conversely, a larger F_G compelled the carriers to keep swirling at the bottom without being entrained. Thus, the carriers could barely be detected, and the drug particles and drug aggregations were released slowly. Since the existence of mucus layers in human bronchi, particles would not be able to move with air flow after deposition. It was suggested that few drug particles or drug aggregations detached from the carriers in gradual inhalation at 30 L/min because the particles and aggregations were almost co-deposited with the carriers.

At 60 L/min, the R_{max} and R_{AUC} of DPIs increased compared with those at 30 L/min. Specifically, the R_{AUC} of drug particles (1.43-fold) and carriers increased, while the R_{AUC} of drug aggregations declined. Larger F_D acted on the particles and accelerated their movement at 60 L/min. More DPIs particles could enter the detector before deposition, which was responsible for the increase in the R_{max} and R_{AUC} of DPIs. In addition, the detachment was facilitated by a larger F_C. More drug particles and drug aggregations could be detached from the carriers. Additionally, the cohesive force of the drug aggregations was overcome by F_C, and the drug aggregations de-agglomerated into drug particles, which

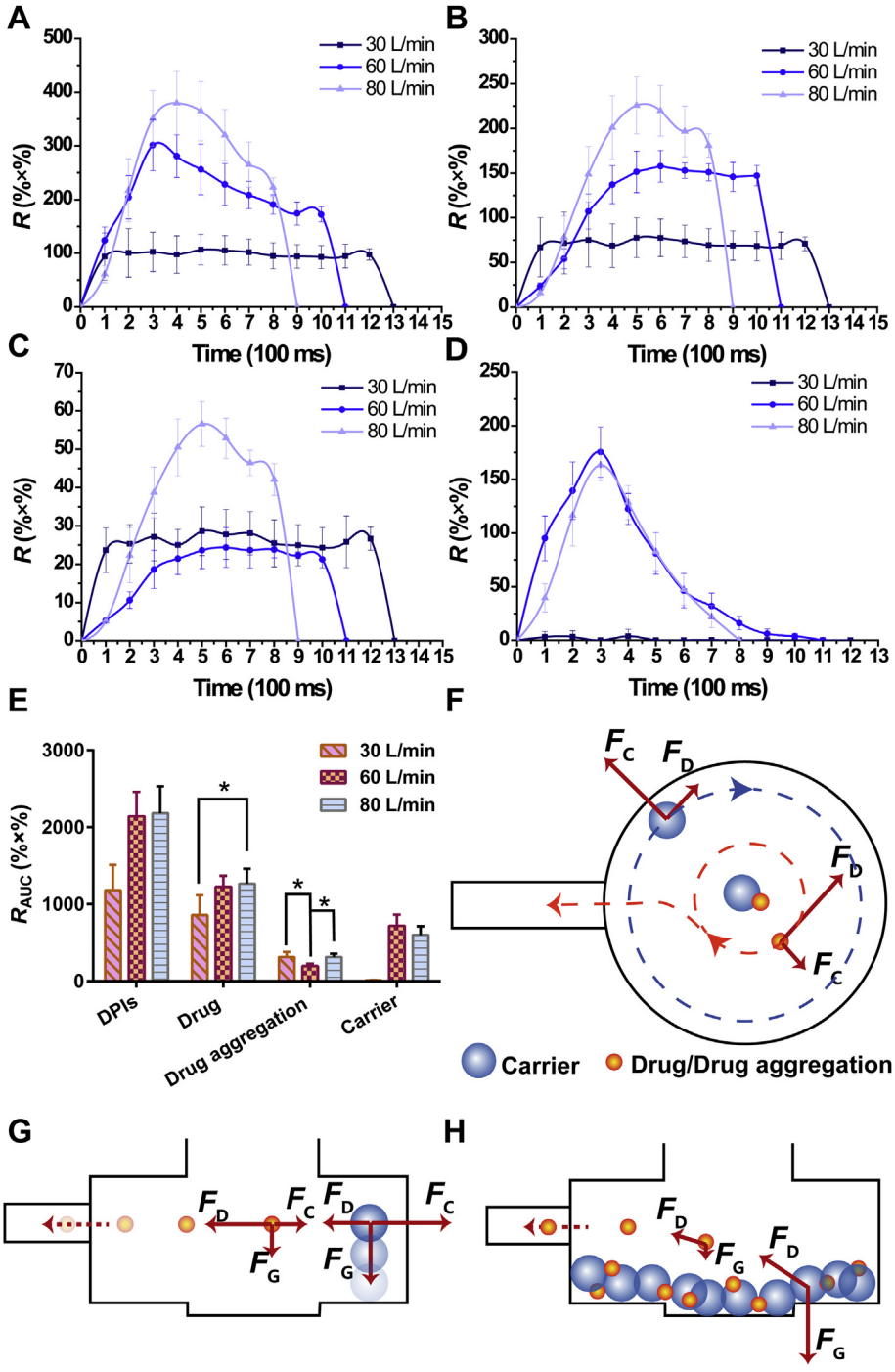

Figure 7 Release profiles and total release amount of conuration C. (A) Release profiles of DPIs; (B) Release profiles of drug; (C) Release profiles of drug aggregation; (D) Release profiles of carrier; (E) Total release amount at different flow rates; (F) Detachment of carrier–drug/drug aggregation due to different F_C; (G) Carrier deposited on the bottom of pre-separator at low U_0 while drug/drug aggregation could be transported to deeper airways; (H) DPIs particles impacted with each other at the bottom of pre-separator (All the data were presented as mean ± SD, $^*P < 0.05$, $n = 3$). U_0, air flow rate; F_C, centrifugal force.

further increased the release of the drug. Therefore, the R_{AUC} of drug increased and the R_{AUC} of drug aggregations decreased.

When U_0 further increased to 80 L/min, there was no significant change ($P > 0.05$) in the R_{AUC} of DPIs. Therein, the R_{AUC} of drug aggregations increased while the R_{AUC} of carriers declined, and the R_{AUC} of drug particles did not change distinctly ($P > 0.05$). As mentioned above, larger F_D and F_C during bursting inhalation resulted in more DPIs reaching the detector and more detachment, respectively. However, the movement locus of carriers was too close to the wall of pre-separator when U_0 was too high. Friction between the particles and wall led to a decrease in the kinetic energy of the carriers, which ultimately resulted in deposition. In addition, the decrease in carrier release caused by deposition was greater than the increase caused by F_D. In contrast,

there was a balance between deposition and detachment of the drug particles. Hence, the R_{AUC} of carriers dropped while the R_{AUC} of drug particles remained stable. The above results were in agreement with a CFD-DEM study, suggesting that an increase in the inhaler dispersion performance occurred at each flow rate increment between 30 and 75 L/min, but no further improvement was observed above 75 L/min[62]. Moreover, the probability of particles impacting each other increased at 80 L/min. The detached drug particles could form aggregates because of impaction, which was responsible for the increase in the R_{AUC} of drug aggregations.

In short, the pre-separator simulated the transportation and detachment processes in the bronchi bifurcation of DPIs after passing through the throat. Compared with artificial throat, the pre-separator produced more efficient detachment of carrier–drug/drug aggregation. The F_C in pre-separator served the same function as bronchi bifurcation. The carriers, drug aggregations and drugs of different particle sizes encountered various F_C that resulted in the occurrence of detachment. The detached drug particles could be efficiently transported into the lower parts of the airways and deposited in the deep pulmonary system. In addition, U_0 played a critical role in the transportation and detachment processes of the DPIs. At low U_0, gradual inhalation mainly led to co-deposition of carriers–drug particles/drug aggregations, since F_G dominated the movement of the particles, while F_C was relatively small. Although high U_0 was beneficial to detachment, excessive U_0 in bursting inhalation would aggravate the deposition and aggregation; thus, the release of the drug decreased. Briefly, 60 L/min possessed the same pulmonary drug delivery efficiency as 80 L/min but easier to generate by patients. Therefore, 60 L/min was the optimal U_0 in the present study.

MMSH was able to realize simultaneous detection of PDPs including fluidization and dispersion, transportation, detachment and deposition within one test. And the mechanism of PDPs in DPIs was fully investigated by MMSH, which could be further applied to various designs and optimizations of DPIs. Thus, more information could be acquired efficiently by MMSH, showing its advantages and innovations over CFD-DEM. For instance, this information was applicable to evaluating the impact of the inhalation breath pattern mimicked by a breath simulator on pulmonary drug delivery efficiency. Furthermore, this research could be used in the design and optimization of inhaler devices. The information about when and where detachment and deposition occurred could be monitored in real time, showing the direction of improvement.

3.4. *In vitro aerosolization performance investigation of DPIs by NGI*

NGI was a widely recognized evaluation approach for the *in vitro* aerosolization performance of DPIs[63–65]. In the present study, the modular concept was also applied in NGI experiments to explore the aerosolization performance of model DPIs under different U_0 in detail. Specifically, the standard NGI configuration (inhaler device, USP throat, pre-separator, stages 1−7 and MOC)[66] and NGI without pre-separator configuration (Supporting Information Fig. S2) were employed to distinguish the different roles of the pre-separator and USP throat in the PDPs of DPIs. In addition, the deposition of carriers was detected in the present study to acquire deeper insight into the PDPs of DPIs. The FPF values, drug and carrier deposition profiles in NGI without/with pre-separator under different U_0 were presented in Fig . 8, and the relevant parameters were shown in Table 3.

For the NGI without pre-separator, the FPF values had significant difference ($P < 0.05$) in various U_0, which increased with increasing U_0 (Fig. 8A). In addition, the FPD values showed the same tendency as FPF. According to the deposition profiles of the drug particles and carriers (Fig. 8A–B), the most distinct deposition was observed in stage 1 (S1). The amount of deposited drug particles in S1 (S1-drug) decreased sharply as U_0 increased, which indicated that the drug particles were further transported and deposited in lower stages (S2−S7), prompting an increase in the FPF values. On the contrary, S1–S7 & MOC-carrier increased with increasing U_0 (Fig. 8B), demonstrating that more carriers participated in further transportation.

According to the results above, a reasonable hypothesis that the FPF values varied with air flow could be conducted. The increased U_0 offered enhanced kinetic energy for DPIs to disperse and fluidize; thus, more particles could be entrained by air flow into lower stages, resulting in higher FPF values. Of note, a linear relationship was determined between the FPF values and the R_{AUC} of drug particles of configuration B by MMSH ($R^2 = 0.8948$, Supporting Information Fig. S3A). However, bronchi bifurcation in the human body[67] resulted in detachment of drug–carrier due to vortex air flow. Therefore, pre-separator should be equipped to simulate the function of bronchi bifurcation for more realistic pulmonary delivery of DPIs.

With regard to NGI with the pre-separator, the FPF values increased remarkably (1.78-fold) as the flow rate increased from 30 to 60 L/min, while there was no significant difference ($P > 0.05$) between those at 60 and 80 L/min (Fig. 8C). The same trend was also found for the FPD values with various air flows. Specifically, most of the drugs and carriers were found in pre-separator (Fig. 8C–D). The drug deposition in the pre-separator (Pre-drug) was up to 65.56 ± 3.52% at 30 L/min and decreased to 50.16 ± 3.02% at 60 L/min. There was no significant difference in pre-drug between 60 and 80 L/min ($P > 0.05$). In addition, more than 93% of the carriers deposited on the pre-separator and the carrier deposition increased with the increase of U_0. While the carrier deposited in the device, adapter and throat decreased with the increasing U_0.

The pre-separator was designed to detach the drug particles from the carriers during DPIs evaluation[66], simulating the function of bronchi bifurcation. The vortex air flow within the pre-separator became stronger with increasing U_0, leading to more violent impaction between DPIs particles. Therefore, the detachment between drug–carrier was more obvious. The detached drug particles were capable of reaching lower stages due to air flow entrainment, which consequently increased the FPF values. However, excessively strong air flow was not essential to the model DPIs and might lead to the aggregation of the drug and untimely deposition of the drug in pre-separator. Therefore, the FPF value at 80 L/min did not increase compared with that at 60 L/min. It is worth noting that a favorable linear relationship between the FPF values and the R_{AUC} of drug particles was demonstrated ($R^2 = 0.9898$, Fig. S3B). Briefly, a desirable correlation was established between the results of NGI and MMSH.

The FPF values of NGI without pre-separator were higher than those of NGI with pre-separator at each U_0. Furthermore, the S1-drug sharply declined when the pre-separator was equipped, and the S2−S7-drug presented the same tendency. In regard to NGI without a pre-separator, more carrier particles took part in the transportation in lower stages, and the drug particles were delivered to lower stages as

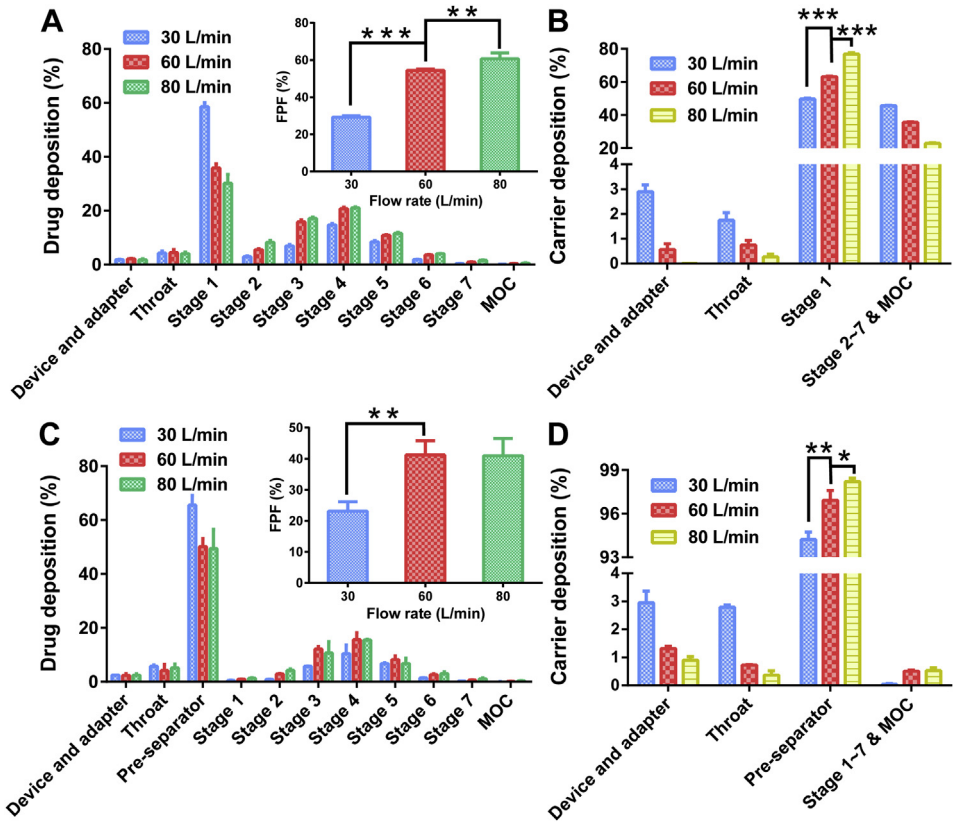

Figure 8 *In vitro* aerosolization performance of model DPIs. (A) Drug deposition profile. Inset was the FPF values of NGI without pre-separator; (B) Carrier deposition profile of NGI without pre-separator; (C) Drug deposition profile. Inset was the FPF values of NGI with pre-separator; (D) Carrier deposition profile of NGI with pre-separator All the data were presented as mean ± SD, $^{*}P < 0.05$, $^{**}P < 0.01$, $^{***}P < 0.005$, $n = 3$. FPF, fine particle fraction; NGI, Next Generation Impactor.

Table 3 MMAD, ED and FPD of NGI with/without pre-separator under different flow rate (the data were presented as mean ± SD, $n = 3$).

Instrument	NGI without pre-separator			NGI with pre-separator		
Flow rate (L/min)	30	60	80	30	60	80
MMAD (μm)	–	3.82 ± 0.07	3.09 ± 0.29	2.91 ± 0.05	2.36 ± 0.05	2.06 ± 0.13
ED (%)	99.04 ± 1.67	99.58 ± 3.28	98.40 ± 2.78	98.71 ± 1.45	98.76 ± 3.09	98.69 ± 1.14
FPD (μg)	122.30 ± 16.08	236.12 ± 10.59	267.84 ± 12.56	86.80 ± 9.63	171.37 ± 18.83	170.82 ± 13.12

–Not applicable.

carrier–drug complexes. Therefore, the FPF values were deceptively high. On the contrary, the pre-separator performed the function of bronchi bifurcation. More drug particles detached from the carriers in pre-separator and were further entrained to lower stages by air flow, while some of the drug particles still adhered to the carriers because of the strong F_I (such as electrostatic force, friction force and adhesive force)[51], resulting in co-deposition with the carriers in pre-separator. Hence, the FPF values decreased with the addition of pre-separator. In sum, the pre-separator played a critical role in determining the pulmonary drug delivery efficiency of DPIs, which was indispensable in NGI tests as well as MMSH experiments. The application of the modular concept in NGI could provide preliminary insight into the PDPs of DPIs and the effect of U_0.

The aerosolization performance of model DPIs was susceptible to U_0. The U_0 of 60 L/min was the optimum for the *in vitro* aerosolization performance of model DPIs, under which obtained highest FPF values. A good correlation was demonstrated between the results of NGI and MMSH. It was indicated that a feasible and credible method that offered a new approach to DPIs PDPs in detail and in real-time was first and successfully developed.

4. Conclusions

The PDPs mechanism of carrier-based DPIs was essential in the design and optimization of DPIs formulations. However, the current evaluation approaches for DPIs could not investigate each PDP of DPIs separately. In the present study, a modular concept was innovatively integrated with Sympatec HELOS to simulate the PDPs of DPIs in inhaler device, throat and tracheal bronchus, respectively. The dispersion, fluidization, transportation, detachment and deposition of DPIs under different U_0

were meticulously explored by the MMSH. Moreover, the mechanism of PDPs in DPIs was discussed in detail. Furthermore, a satisfactory correlation between the results of the MMSH and NGI was built up. In summary, a credible and time-saving method that could explore the PDPs of DPIs in detail and in real-time was first and successfully developed. The MMSH presented great potential to become an efficient approach for the DPIs formulation design and optimization. Furthermore, the MMSH was subjected to an ongoing study to investigate the effects of the powder properties of carriers (such as particle size, surface morphology/roughness and electrical properties) and the types of devices on the delivery process of pulmonary DPIs, which is pioneering work on the innovation and development of DPIs.

Acknowledgments

This paper was funded by the National Natural Science Foundation of China (81673375 and 81703431), the Science and Technology Foundation Guangzhou (201509030006, China) and the National Students Innovation Training Program of China (201901390). The authors thanked Sympatec GmbH (Clausthal-Zellerfeld, Germany) for the technical support and Majesty Packaging Systems Co., Ltd. (Guangdong, China) for making the connector between artificial throat and Sympatec HELOS.

Author contributions

Xuejuan Zhang and Yingtong Cui designed the experiment, analyzed the data and wrote the manuscript. Yingtong Cui, Xiao Yue, Guanlin Wang, Ruifeng Liang and Ziyu Zhao helped perform the experiments. Ying Huang and Xuejuan Zhang revised the manuscript and the artworks. Ying Huang, Jianfang Geng, Xin Pan and Chuanbin Wu were responsible for fund-seeking, supervision and proof-reading.

Conflicts of interest

The authors have no conflicts of interest to declare.

Appendix A. Supporting information

Supporting data to this article can be found online at https://doi.org/10.1016/j.apsb.2020.02.013.

References

1. Li L, Leung SSY, Gengenbach T, Yu J, Gao GF, Tang P, et al. Investigation of L-leucine in reducing the moisture-induced deterioration of spray-dried salbutamol sulfate power for inhalation. *Int J Pharm* 2017;**530**:30−9.
2. Pessôa CL, Mattos MJ, Alho AR, Fischmann MM, Haerdy BM, Côrtes AC, et al. Most frequent errors in inhalation technique of patients with asthma treated at a tertiary care hospital. *Einstein (Sao Paulo)* 2019;**17**:eAO4397.
3. Muralidharan P, Hayes D, Mansour HM. Dry powder inhalers in COPD, lung inflammation and pulmonary infections. *Expet Opin Drug Deliv* 2015;**12**:947−62.
4. Kozáková J, Altay A, Ždímal V, Mašková L, Sonvico F, Quarta E, et al. Dry powder inhaler of colistimethate sodium for lung infections in cystic fibrosis: optimization of powder construction. *Drug Dev Ind Pharm* 2019;**45**:1664−73.
5. Zhang T, Chen Y, Ge Y, Hu Y, Li M, Jin Y. Inhalation treatment of primary lung cancer using liposomal curcumin dry powder inhalers. *Acta Pharm Sin B* 2018;**8**:440−8.
6. Kim ES, Plosker GL. AFREZZA® (insulin human) inhalation powder: a review in diabetes mellitus. *Drugs* 2015;**75**:1679−86.
7. Valdes J, Shipley T, Rey JA. Loxapine inhalation powder (adasuve): a new and innovative formulation of an antipsychotic treatment for agitation. *P T* 2014;**39**:621−3. 648.
8. Rudén J, Frenning G, Bramer T, Thalberg K, An J, Alderborn G. Linking carrier morphology to the powder mechanics of adhesive mixtures for dry powder inhalers *via* a blend-state model. *Int J Pharm* 2019;**561**:148−60.
9. Rudén J, Frenning G, Bramer T, Thalberg K, Alderborn G. Relationships between surface coverage ratio and powder mechanics of binary adhesive mixtures for dry powder inhalers. *Int J Pharm* 2018;**541**:143−56.
10. Zhao Z, Zhang X, Cui Y, Huang Y, Huang Z, Wang G, et al. Hydroxypropyl-β-cyclodextrin as anti-hygroscopicity agent in amorphous lactose carriers for dry powder inhalers. *Powder Technol* 2019;**358**:29−38.
11. Zhang X, Zhao Z, Cui Y, Liu F, Huang Z, Huang Y, et al. Effect of powder properties on the aerosolization performance of nanoporous mannitol particles as dry powder inhalation carriers. *Powder Technol* 2019;**358**:46−54.
12. Faulhammer E, Zellnitz S, Wutscher T, Stranzinger S, Zimmer A, Paudel A. Performance indicators for carrier-based DPIs: carrier surface properties for capsule filling and API properties for *in vitro* aerosolisation. *Int J Pharm* 2018;**536**:326−35.
13. Peng T, Zhang X, Huang Y, Zhao Z, Liao Q, Xu J, et al. Nanoporous mannitol carrier prepared by non-organic solvent spray drying technique to enhance the aerosolization performance for dry powder inhalation. *Sci Rep* 2017;**7**:46517.
14. Clarke SW. Chapter 1 - anatomy and physiology of the human lung: aspects relevant to aerosols. In: Clarke SW, Pavia D, editors. *Aerosols and the lung: clinical and experimental aspects*. London: Butterworth-Heinemann; 1984. p. 1−18.
15. Healy AM, Amaro MI, Paluch KJ, Tajber L. Dry powders for oral inhalation free of lactose carrier particles. *Adv Drug Deliv Rev* 2014;**75**:32−52.
16. Zhao Z, Huang Z, Zhang X, Huang Y, Cui Y, Ma C, et al. Low density, good flowability cyclodextrin-raffinose binary carrier for dry powder inhaler: anti-hygroscopicity and aerosolization performance enhancement. *Expet Opin Drug Deliv* 2018;**15**:443−57.
17. Jetzer MW, Morrical BD, Schneider M, Edge S, Imanidis G. Probing the particulate microstructure of the aerodynamic particle size distribution of dry powder inhaler combination products. *Int J Pharm* 2018;**538**:30−9.
18. Grasmeijer F, Grasmeijer N, Hagedoorn P, Frijlink HW, de Boer AH. Recent advances in the fundamental understanding of adhesive mixtures for inhalation. *Curr Pharmaceut Des* 2015;**21**:5900−14.
19. Shalash AO, Elsayed MMA. A new role of fine excipient materials in carrier-based dry powder inhalation mixtures: effect on deagglomeration of drug particles during mixing revealed. *AAPS PharmSciTech* 2017;**18**:2862−70.
20. Kinnunen H, Hebbink G, Peters H, Shur J, Price R. An investigation into the effect of fine lactose particles on the fluidization behaviour and aerosolization performance of carrier-based dry powder inhaler formulations. *AAPS PharmSciTech* 2014;**15**:898−909.
21. Zhou Q, Tong Z, Tang P, Yang R, Chan HK. CFD analysis of the aerosolization of carrier-based dry powder inhaler formulations. *AIP Conf Proc* 2013;**1542**:1146−9.
22. Leung CM, Tong Z, Zhou QT, Chan JG, Tang P, Sun S, et al. Understanding the different effects of inhaler design on the aerosol performance of drug-only and carrier-based DPI formulations. Part 1: grid structure. *AAPS PharmSciTech* 2016;**18**:1159−67.

23. Leung SS, Tang P, Zhou Q, Tong Z, Leung C, Decharaksa J, et al. De-agglomeration effect of the *US pharmacopeia* and Alberta throats on carrier-based powders in commercial inhalation products. *AAPS PharmSciTech* 2015;**17**:1407−16.
24. Mahler DA. Peak inspiratory flow rate as a criterion for dry powder inhaler use in chronic obstructive pulmonary disease. *Ann Am Thorac Soc* 2017;**14**:1103−7.
25. Holmes MS, Seheult J, Geraghty C, D'Arcy S, Costello RW, Reilly RB. Using acoustics to estimate inspiratory flow rate and drug removed from a dry powder inhaler. *Conf Proc IEEE Eng Med Biol Soc* 2013;**2013**:6866−9.
26. Zeman KL, Wu J, Bennett WD. Targeting aerosolized drugs to the conducting airways using very large particles and extremely slow inhalations. *J Aerosol Med Pulm Drug Deliv* 2010;**23**:363−9.
27. Floroiu A, Klein M, Krämer J, Lehr CM. Towards standardized dissolution techniques for *in vitro* performance testing of dry powder inhalers. *Dissolution Technol* 2018;**25**:6−18.
28. Kurumaddali A, Christopher D, Sandell D, Strickland H, Morgan B, Bulitta J, et al. Cascade impactor equivalence testing: comparison of the performance of the modified chi-square ratio statistic (mCSRS) with the original CSRS and EMA's average bioequivalence approach. *AAPS PharmSciTech* 2019;**20**:249.
29. Jafar END, Hamishehkar H, Valizadeh. Development of dry powder inhaler formulation loaded with alendronate solid lipid nanoparticles: solid-state characterization and aerosol dispersion performance. *Drug Dev Ind Pharm* 2015;**41**:1431−7.
30. Zhou QT, Tong Z, Tang P, Citterio M, Yang R, Chan HK. Effect of device design on the aerosolization of a carrier-based dry powder inhaler—a case study on Aerolizer® Foradile®. *AAPS PharmSciTech* 2013;**15**:511−22.
31. Sommerfeld M, Cui Y, Schmalfuß S. Potential and constraints for the application of CFD combined with Lagrangian particle tracking to dry powder inhalers. *Eur J Pharmaceut Sci* 2019;**128**:299−324.
32. Li J, Agarwal RK, Zhou L, Yang B. Investigation of a bubbling fluidized bed methanation reactor by using CFD-DEM and approximate image processing method. *Chem Eng Sci* 2019;**207**:1107−20.
33. Zhou M, Wang S, Kuang S, Luo K, Fan J, Yu A. CFD-DEM modelling of hydraulic conveying of solid particles in a vertical pipe. *Powder Technol* 2019;**354**:893−905.
34. Yang J, Wu CY, Adams M. Three-dimensional DEM-CFD analysis of air-flow-induced detachment of API particles from carrier particles in dry powder inhalers. *Acta Pharm Sin B* 2014;**4**:52−9.
35. Tang P, Kwok PC, Tong Z, Yang R, Raper JA, Chan HK. Does the *United States Pharmacopeia* throat introduce de-agglomeration of carrier-free powder from inhalers?. *Pharm Res (N Y)* 2012;**29**:1797−807.
36. Modugno C, Paterson AHJ, McLeod J. Lactose caking: influence of the particle size distribution and the water content. *Procedia Eng* 2015;**102**:114−22.
37. Hagedoorn P, Bawary W, Frijlink HW, Grasmeijer F. A comparative analysis of changes in pMDI drug dose delivery before and after detergent coating using five antistatic valved holding chambers. *J Aller Cl Imm-Pract* 2020;**8**:1124−5.
38. Pankewitz A, Behrens C, Kesten U, Park YJ. Particle size and shape analysis the key to success in metal powder production. *Mater Sci Forum* 2007;**534**−**536**:101−4.
39. McDonnell KA, English NJ, Stallard CP, Rahman M, Dowling DP. Fabrication of nano-structured TiO2 coatings using a microblast deposition technique. *Appl Surf Sci* 2013;**275**:316−23.
40. Hoffmann S, Koos E, Willenbacher N. Using capillary bridges to tune stability and flow behavior of food suspensions. *Food Hydrocolloids* 2014;**40**:44−52.
41. Zhou Z, Buchanan F, Mitchell C, Dunne N. Printability of calcium phosphate: calcium sulfate powders for the application of tissue engineered bone scaffolds using the 3D printing technique. *Mater Sci Eng C* 2014;**38**:1−10.
42. Lexmond AJ, van der Wiel E, Hagedoorn P, Bult W, Frijlink HW, ten Hacken NH, et al. Adenosine dry powder inhalation for bronchial challenge testing, part 2: proof of concept in asthmatic subjects. *Eur J Pharm Biopharm* 2014;**88**:148−52.
43. Patil S, Mahadik A, Nalawade P, More P. Crystal engineering of lactose using electrospray technology: carrier for pulmonary drug delivery. *Drug Dev Ind Pharm* 2017;**43**:2085−91.
44. Onoue S, Kuriyama K, Uchida A, Mizumoto T, Yamada S. Inhalable sustained-release formulation of glucagon: *in vitro* amyloidogenic and inhalation properties, and *in vivo* absorption and bioactivity. *Pharm Res (N Y)* 2011;**28**:1157−66.
45. Lexmond AJ, Hagedoorn P, van der Wiel E, ten Hacken NH, Frijlink HW, de Boer AH. Adenosine dry powder inhalation for bronchial challenge testing, part 1: inhaler and formulation development and *in vitro* performance testing. *Eur J Pharm Biopharm* 2014;**86**:105−14.
46. de Boer AH, Gjaltema D, Hagedoorn P, Schaller M, Witt W, Frijlink HW. Design and application of a new modular adapter for laser diffraction characterization of inhalation aerosols. *Int J Pharm* 2002;**249**:233−45.
47. Kou X, Wereley ST, Heng PW, Chan LW, Carvajal MT. Powder dispersion mechanisms within a dry powder inhaler using microscale particle image velocimetry. *Int J Pharm* 2016;**514**:445−55.
48. Le VN, Robins E, Flament MP. Air permeability of powder: a potential tool for dry powder inhaler formulation development. *Eur J Pharm Biopharm* 2010;**76**:464−9.
49. Wirth KE, Linsenbühler M. Electrostatically supported mixing of fine grained particles. *China Particuol* 2005;**3**:94−8.
50. Hoppentocht M, Hagedoorn P, Frijlink HW, de Boer AH. Technological and practical challenges of dry powder inhalers and formulations. *Adv Drug Deliv Rev* 2014;**75**:18−31.
51. Begat P, Morton DA, Staniforth JN, Price R. The cohesive-adhesive balances in dry powder inhaler formulations I: direct quantification by atomic force microscopy. *Pharm Res (N Y)* 2004;**21**:1591−7.
52. Tan SB, Newton JM. Influence of capsule dosator wall texture and powder properties on the angle of wall friction and powder-wall adhesion. *Int J Pharm* 1990;**64**:227−34.
53. Frijlink HW, De Boer AH. Dry powder inhalers for pulmonary drug delivery. *Expet Opin Drug Deliv* 2004;**1**:67−86.
54. Dalrymple P, Griffiths R. Force, mass and acceleration. *Anaesth Intensive Care Med* 2005;**6**:294.
55. Milenkovic J, Alexopoulo AH, Kiparissides C. Airflow and particle deposition in a dry powder inhaler: an integrated CFD approach. *Adv Intel Systems Computing* 2014;**256**:127−40.
56. Weers J. Regional deposition of particles within the respiratory tract should be linked to impaction parameter, not aerodynamic size. *J Aerosol Med Pulm Drug Deliv* 2018;**31**:116−8.
57. Weers J, Clark A. The impact of inspiratory flow rate on drug delivery to the lungs with dry powder inhalers. *Pharm Res (N Y)* 2017;**34**:507−28.
58. de Boer AH, Chan HK, Price R. A critical view on lactose-based drug formulation and device studies for dry powder inhalation: which are relevant and what interactions to expect?. *Adv Drug Deliv Rev* 2012;**64**:257−74.
59. Hadinoto K, Curtis JS. Reynolds number dependence of gas-phase turbulence in particle-laden flows: effects of particle inertia and particle loading. *Powder Technol* 2009;**195**:119−27.
60. Bhattacharya J, Matthay MA. Regulation and repair of the alveolar-capillary barrier in acute lung injury. *Annu Rev Physiol* 2013;**75**:593−615.
61. Khalili SF, Ghanbarzadeh S, Nokhodchi A, Hamishehkar H. The effect of different coating materials on the prevention of powder bounce in the next generation impactor. *Res Pharm Sci* 2018;**13**:283−7.
62. Coates MS, Chan HK, Fletcher DF, Raper JA. Influence of air flow on the performance of a dry powder inhaler using computational and experimental analyses. *Pharm Res (N Y)* 2005;**22**:1445−53.
63. Qiu Y, Man RC, Liao Q, Kung KL, Chow MY, Lam JKW. Effective mRNA pulmonary delivery by dry powder formulation of PEGylated synthetic KL4 peptide. *J Contr Release* 2019;**314**:102−15.

64. Lababidi N, Ofosu Kissi E, Elgaher WA, Sigal V, Haupenthal J, Schwarz BC, et al. Spray-drying of inhalable, multifunctional formulations for the treatment of biofilms formed in cystic fibrosis. *J Contr Release* 2019;**314**:62−71.
65. Dolovich MB, Kuttler A, Dimke TJ, Usmani OS. Biophysical model to predict lung delivery from a dual bronchodilator dry-powder inhaler. *Int J Pharm X* 2019;**1**:100018.
66. Marple VA, Roberts DL, Romay FJ, Miller NC, Truman KG, Van Oort M, et al. Next generation pharmaceutical impactor (a new impactor for pharmaceutical inhaler testing). Part I: design. *J Aerosol Med* 2003;**16**:283−99.
67. Lee HG, Kim DW, Park CW. Dry powder inhaler for pulmonary drug delivery: human respiratory system, approved products and therapeutic equivalence guideline. *J Pharm Inv* 2018;**48**:603−16.